NREL/SR-520-22362 • UC Category: 1260 • DE97000102

Research on High-Bandgap Materials and Amorphous Silicon-Based Solar Cells

Annual Technical Report
15 May 1995 - 15 May 1996

Schiff, E.A.; Gu, Q.; Jiang, L.; and Rao, P.
Syracuse University
Syracuse, New York

NREL technical monitor: B. von Roedern

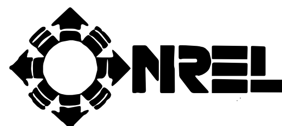

National Renewable Energy Laboratory
1617 Cole Boulevard
Golden, Colorado 80401-3393
A national laboratory of the U.S. Department of Energy
Managed by Midwest Research Institute
for the U.S. Department of Energy
under Contract No. DE-AC36-83CH10093

Prepared under Subcontract No. XAN-4-13318-06

January 1997

This publication was reproduced from the best available camera-ready copy
submitted by the subcontractor and received no editorial review at NREL.

NOTICE

This report was prepared as an account of work sponsored by an agency of the United States government. Neither the United States government nor any agency thereof, nor any of their employees, makes any warranty, express or implied, or assumes any legal liability or responsibility for the accuracy, completeness, or usefulness of any information, apparatus, product, or process disclosed, or represents that its use would not infringe privately owned rights. Reference herein to any specific commercial product, process, or service by trade name, trademark, manufacturer, or otherwise does not necessarily constitute or imply its endorsement, recommendation, or favoring by the United States government or any agency thereof. The views and opinions of authors expressed herein do not necessarily state or reflect those of the United States government or any agency thereof.

Available to DOE and DOE contractors from:
Office of Scientific and Technical Information (OSTI)
P.O. Box 62
Oak Ridge, TN 37831
Prices available by calling (423) 576-8401

Available to the public from:
National Technical Information Service (NTIS)
U.S. Department of Commerce
5285 Port Royal Road
Springfield, VA 22161
(703) 487-4650

Printed on paper containing at least 50% wastepaper, including 20% postconsumer waste

Preface

This research project has three broad objectives:

- We seek a deeper understanding of the open circuit voltage V_{OC} in amorphous silicon based solar cells, and in particular for cells employing wide bandgap modification of amorphous silicon as their absorber layer. Our technical approach has emphasized the development of electroabsorption measurements as a tool for probing the built-in potential of a-Si:H based solar cells.

- We are working to improve V_{OC} in wide bandgap cells by searching for superior materials for the *p*-type "window layer" of the cell.

- We seek to improve our understanding of the fundamental electron and hole photocarrier transport processes in the materials used for amorphous silicon based solar cells.

In addition to the authors of this report, we have reported work which includes the contributions of several collaborators, in particular Reinhard Schwarz, Stefan Grebner, and Fuchao Wang of the Technical University of Munich, and Richard Crandall, Eugene Iwanicszko, Brent Nelson, and Qi Wang of the National Renewable Energy Laboratory, Subhendu Guha and Jeff Yang at United Solar Systems Corp., and Xunming Deng at Energy Conversion Devices, Inc.,

We have also benefitted from the cooperation and interest of several other scientists and organizations. In particular we thank Christopher Wronski at Pennsylvania State University, Steve Hegedus at the Institute of Energy Conversion, University of Delaware, and Murray Bennett at Solarex Corp. Thin Films Division.

Summary

- We have developed a technique based on electroabsorption measurements for obtaining quantitative estimates of the built-in potential in a-Si:H based heterostructure solar cells incorporating microcrystalline or a-SiC:H *p* layers. This heterostructure problem has been a major limitation in application of the electroabsorption technique. The new technique only utilizes measurements from a particular solar cell, and is thus a significant improvement on earlier techniques requiring measurements on auxiliary films.

- Using this new electroabsorption technique, we confirmed previous estimates of $V_{bi} \approx 1.0$ V in a-Si:H solar cells with "conventional" intrinsic layers and either microcrystalline or a-SiC:H *p* layers. Interestingly, our first measurements on high V_{oc} cells grown with "high hydrogen dilution" intrinsic layers yield a much larger value for $V_{bi} \approx 1.3$ V. We speculate that these results are evidence for a significant interface dipole at the *p/i* heterostructure interface. Although we believe that interface dipoles rationalize several previously unexplained effects on a-Si:H based cells, they are not currently included in models for the operation of a-Si:H based solar cells.

- We have made extensive measurements of hole mobilities in hot-wire deposited a-Si:H. Some of the hot-wire samples yielded standard hole drift mobilities up to five times higher than found in conventional plasma-deposited a-Si:H. We note that the group at Electrotechnical Laboratory in Japan has claimed even larger hole drift mobilities for their materials deposited in a triode plasma reactor.

- We have significantly clarified the relationship of ambipolar diffusion length measurements to hole drift mobilities in a-Si:H. The ambipolar diffusion length L_{amb} is arguably the single most influential parameter in assessing the potential of materials for incorporation as absorbers in a-Si:H based solar cells. We show how L_{amb} can be predicted from hole drift mobilities and the recombination response time of a-Si:H materials. The results are also of interest because they confirm the Einstein relation between diffusion and drift of carriers for disordered materials such as a-Si:H. The Einstein relation is assumed to be valid in device modeling, but this validity had not been established either experimentally or theoretically prior to our work.

- We have completed a survey of thin BP:H and BPC:H films prepared by plasma deposition using phosphine, diborane, tri-methylboron, and hydrogen as precursor gases. The objective of this research has been to find out whether such films might offer a superior window layer film for application to wide bandgap a-Si solar cells. The research has shown good optical properties in a-BP:H films; our films do not have promising electrical properties, and we have suspended this line of research. Most of our research was described in our previous reports, and will not be included again here.

Phase II Publications Acknowledging This Subcontract

1. "Two-layer model for electroabsorption and built-in potential measurements on a-Si:H *pin* solar cells," Lin Jiang and E. A. Schiff, in *Amorphous Silicon Technology-1996*, edited by M. Hack, *et al* (Materials Research Society, Pittsburgh, 1996), *in press*.

2. "Non-Gaussian Transport Measurements and the Einstein Relation in Amorphous Silicon," Qing Gu, E. A. Schiff, S. Grebner, F. Wang, and R. Schwarz, *Phys. Rev. Lett.* **76**, 3196 (1996).

3. "Field collapse due to bandtail charge in amorphous silicon solar cells," Qi Wang, R. S. Crandall, and E. A. Schiff, in *Conference Record of the 21st Photovoltaics Specialists Conference* (IEEE, 1996), 1113.

4. "Fundamental transport mechanisms and high-field mobility measurements in amorphous silicon," Qing Gu, E. A. Schiff, J-B. Chevrier, and B. Equer, *J. Non-Cryst. Solids* (1996), *in press*.

Table of Contents

Preface 2

Summary 2

Phase II Publications Acknowledging This Subcontract 3

Table of Contents 4

Table of Figures 5

Electroabsorption measurements and built-in potentials 6

Introduction 6

Summary of Heterostructure Model for Electroabsorption 8

Experimental Results on Cells with Microcrystalline *p* Layers 9

Interface Dipole Hypothesis 10

Heterostructure Model for Electroabsorption: Details 12

Hole Drift Mobility in Hydrogenated Amorphous Silicon Deposited Using the Hot-Wire Method 14

Introduction 14

Time-of-Flight Measurements 14

Specimens and Instruments 14

Time-of-flight measurements 15

Results 17

Relationship of Ambipolar Diffusion Length Measurements and Hole Drift Mobilities in a-Si:H 18

References 22

Table of Figures

Fig. 1. Modulated electroabsorption signal as a function of the bias potential across the "standard" solar cell. ___ 6

Fig. 2. Wavelength dependence of the electroabsorption parameter V_0 for four different types of a-Si:H based diode structure. ___ 7

Fig. 3. Diagram of the potential profile in a heterostructure *pin* solar cell, illustrating band offsets and an interface dipole. ___ 8

Fig. 4. Plot of the normalized, second harmonic electroabsorption signal δT_{2f} for three different wavelengths as a function of reciprocal capacitance in the standard cell; the data are generated by varying the reverse bias across the cell. ___ 10

Fig. 5. Electroabsorption coefficients α_i'' and α_p'' as a function of wavelength obtained for a-Si:H and for μc-Si:H:B obtained in two types of cell (with standard and strongly H-diluted intrinsic layers). The graph illustrates how the built-in potential is estimated from electroabsorption. ___ 11

Fig. 6. Normalized transient photocurrents $i(t)d^2/Q_0V$ and charges $Q(t)d^2/Q_0V$ for holes measured in a sample of hot-wire a-Si:H at several temperatures ($\lambda = 590$ nm and constant electric field of 69.5 kV/cm). ___ 16

Fig. 7. Plot of average hole drift mobility μ as a function of reciprocal temperature $1/T$ in conventional and hot-wire a-Si:H; the hot-wire specimen has a *larger* hole mobility. ___ 17

Fig. 8. Summary of hole drift mobility at 298 K evaluated at $L/E = 2 \times 10^{-9}$ cm^2/V as a function of bandgap. The highest points are reported recently by Ganguly *et al.* ___ 18

Fig. 9: Diagram of the time-evolution of hole drift and diffusion in a-Si:H, indicating their relationship to time-of-flight and ambipolar diffusion length measurements. ___ 19

Fig. 10. Correlation of the hole diffusion coefficient D_h with the "Einstein normalized" hole drift mobility $(kT/q)\mu_h$. The Einstein relation $D_h = (kT/q)\mu_h$ is indicated by the solid line, and is in fair agreement with the measurements. ___ 20

Electroabsorption measurements and built-in potentials

We present a technique for using modulated electroabsorption measurements to determine the built-in potential in semiconductor heterojunction devices. The technique exploits a simple relationship between the second-harmonic electroabsorption signal and the capacitance of such devices. We apply this technique to hydrogenated amorphous silicon (a-Si:H) based solar cells incorporating microcrystalline Si p^+ layers. For one set of cells with a conventional plasma-deposited intrinsic layer we obtain a built-in potential of 0.98±0.04 V; for cells with an intrinsic layer deposited using strong hydrogen-dilution we obtain 1.25±0.04 V. We speculate that interface dipoles between the p^+ and intrinsic layers significantly influence the built-in potential.

Introduction

The internal electric fields of amorphous silicon (a-Si:H) based *pin* solar cells are crucial to their operation as photocarrier collectors. The *built-in electrostatic potential* V_{bi} established by these fields is thus one of a cell's important device parameters. One promising approach to illustrating and estimating V_{bi} exploits electroabsorption measurements: by measuring the transmittance or reflectance of the cell as a function of an external potential V, an inference of the built-in potential can be made (Nonomura, Okamoto, and Hamakawa, 1983; Wang, Schiff, and Hegedus, 1994; Campbell, Jowick, and Parker, 1995; Jiang and Schiff, 1996; Jiang, Wang, Schiff, Guha, Yang, and Deng, 1996).

Some corresponding measurements are presented in Fig. 1. The transmittance T of a cell is modulated by a sinusoidal potential of amplitude δV; the transmittance modulation δT_{1f} in phase with δV is then plotted as

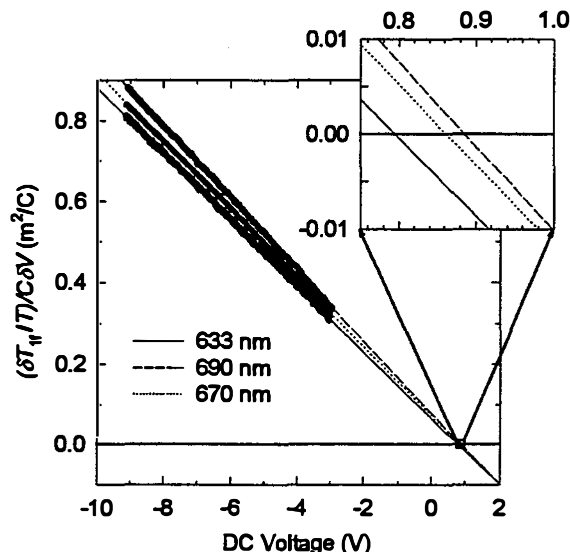

Fig. 1. Modulated electroabsorption signal as a function of the bias potential across the "standard" solar cell. The voltage-axis intercept has been used to estimate the built-in potential of the solar cell. Measurements at three laser wavelengths are illustrated, and show (cf. inset) that the intercept depends slightly on the measuring wavelength.

a function of the external DC potential V. One sees that the transmittance modulation δT_{1f} is quite linear with the external potential. The linearity is a consequence of the fact that electroabsorption in non-crystalline materials is quadratic in electric field, and hence δT_{1f} ends up being proportional to $\delta V(V-V_{bi})$. The regression lines through the measurements intersect the horizontal axis near $V = 1.0$ Volts, which is an estimate of the built-in potential of this cell. The slopes of the lines indicate the strength of the electroabsorption effect at each wavelength.

As initially reported by Wang, Schiff, and Hegedus (1994), extensive signal averaging of electroabsorption measurements reveals a systematic dependence of this intercept upon wavelength; the effect is evident in the inset of Fig. 1. Wang, *et al* proposed that this wavelength-dependence is a heterostructure effect, since differing layers have differing wavelength dependences to their electroabsorption. The solar cells studied by Wang, *et al*, had a-Si:H intrinsic and n^+ layers, and an a-SiC:H p^+ layers; in the present work the a-Si:H cells have microcrystalline (not amorphous) p^+ layers.

We present measurements of the wavelength-dependence of the electroabsorption intercept V_0 in Fig. 2 for a variety of a-Si:H based diodes. A quantitative interpretation for these measurements will be given shortly. Here we note primarily that the interpretation of the wavelength-dependence as a heterostructure effect is reasonably consistent with the measurements on a-Si:H *nim* Schottky barrier diodes. If the wavelength-dependence is to be associated with voltage drops in a p^+ material which is dissimilar to the intrinsic layer, then one expects a much reduced effect in a Schottky barrier in which the p^+ layer is replaced by a metal. Within the metal the potential drops should be insignificant. As can be seen in the figure, the Schottky barrier structure shows a much reduced wavelength-dependence.

More generally, the "slope" of the wavelength dependence is determined by a competititon between the

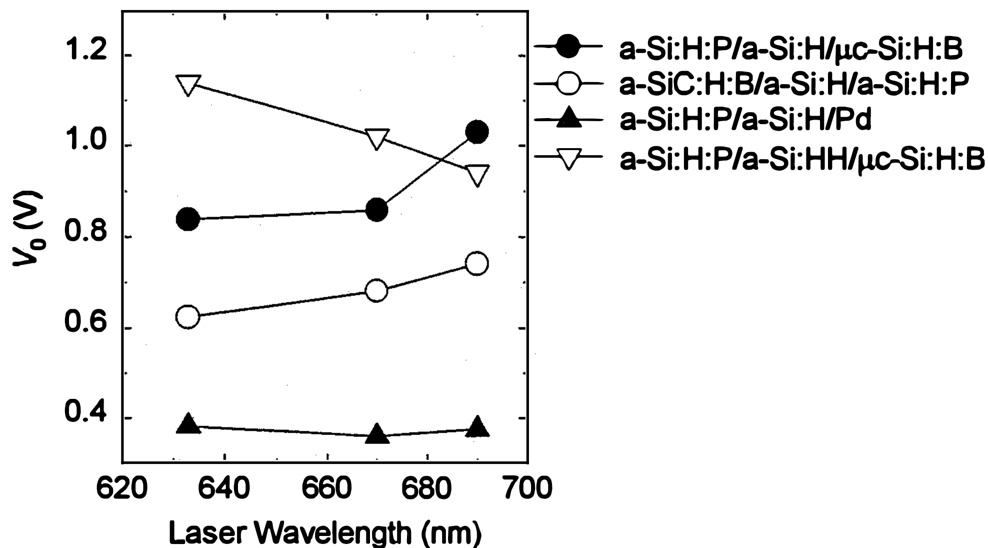

Fig. 2. Wavelength dependence of the electroabsorption parameter V_0 for four different types of a-Si:H based diode structure. The symbol a-Si:HH denotes a-Si:H plasma-deposited from silane using high hydrogen dilution. In the simplest model V_0 is wavelength-independent, and is identified as the built-in potential. Note that the wavelength-dependence is weakest for the Schottky barrier diode with no p^+ layer, suggesting that the wavelength dependence is associated with the varying p^+ layers.

electroabsorption spectra in the p^+ and intrinsic layers. Very roughly speaking, when the p^+ layer has a significantly larger bandgap than the i layer, there is a tendency towards larger values for V_0 for longer wavelengths, where the contribution of the p^+ layer becomes less important. As the i layer bandgap is widened, or the p^+ layer bandgap narrowed, the reverse effect occurs, as for the strongly hydrogen diluted intrinsic layer in Fig. 1. We note that quite similar ideas were used recently by Campbell, *et al* (1995), to interpret electroabsorption measurements on electroluminescent organic heterostructure diodes.

This heterostructure effect undermines efforts to measure V_{bi} quantitatively using electroabsorption. Here we report on a procedure which we believe resolves this difficulty for a-Si:H based solar cells and related devices. We apply the procedure to two types of *nip* solar cells having similar n^+ and p^+ layers, but differing a-Si:H intrinsic layers. In the simplest possible picture the built-in potential is determined by the difference in the Fermi levels of the n^+ and p^+ layers, and should be independent of the intrinsic layer; our estimate of V_{bi} increased from 0.98 to 1.25 V when the intrinsic layer was plasma-deposited using strong hydrogen dilution.

Summary of Heterostructure Model for Electroabsorption

We first describe the model we use for electroabsorption in a *pin* solar cell with a-Si:H n^+ and intrinsic layers and a microcrystalline p^+ layer. In the upper portion of Fig. 3 we show a schematic illustration of the amplitude of the sinusoidally modulated electric field δE. As illustrated, we assumed that this modulation field is uniform across the intrinsic layer, and that it extends only across a depletion zone of the p^+ layer. We also simplified the analysis by neglecting potential drops within the n^+ layer of the cell.

The lower portion of Fig. 3 illustrates the steady-state profile of the conduction band and valence bandedges E_C and E_V; only the solid black curves are important at present. This figure indicates the band-bending eV_p and eV_i in the p^+ and intrinsic layers, respectively. The built-in potential is defined as $V_{bi} = V_p + V_i$. We discuss further details of this figure subsequently.

The electric field dependent absorption in disordered materials is typically quadratic in field $\alpha(\lambda, E) = \alpha^0(\lambda) + \alpha''(\lambda)E^2$; α'' is the *electroabsorption coefficient* of the material. For a sinusoidal

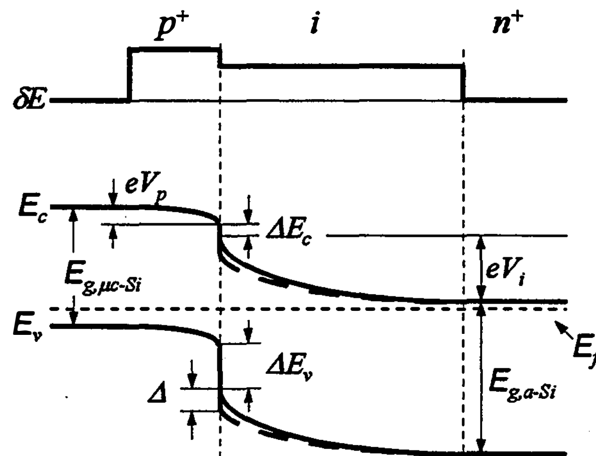

Fig. 3. δE is the amplitude of the modulated electric field across a *pin* solar cell with a microcrystalline p+ layer. The lower portion indicates the conduction and valence bandedges E_c and E_v across the cell, including band bending in the $p+$ and intrinsic layers, band offsets, and an interface dipole Δ.

modulation of amplitude δV, there will be corresponding transmittance modulations δT_{1f} and δT_{2f} at the fundamental and the second harmonic of the modulation frequency, respectively. We measure these signals as a function of a reverse bias potential V across the cell. Reverse-biasing the cell also increases the width of the depletion zone within the p^+ layer, leading to a decrease in the capacitance $C(V)$ of the cell.

The electroabsorption signals δT_{1f} and δT_{2f} can be obtained from analysis of this model; the derivations are given elsewhere. The second-harmonic signal is particularly important in the present, 2-layer system:

$$\frac{\delta T_{2f}/T}{(C(V)\delta V)^2}=\frac{\left(\alpha_p''(\lambda)/\varepsilon_p\right)}{2\varepsilon_0 C(V)}+\frac{\left(\alpha_i''(\lambda)/\varepsilon_i-\alpha_p''(\lambda)/\varepsilon_p\right)}{2\varepsilon_0\left(\varepsilon_i\varepsilon_0/d_i\right)} \tag{1}$$

d_i is the thickness of the cell's intrinsic layer; ε_i and ε_p are the dielectric constants of the intrinsic and p^+ layers, respectively. $C(V)$ refers to the area-normalized capacitance measured at the fundamental modulation frequency. Note that a linear regression of the normalized second harmonic signal against the reciprocal capacitance of the cell yields electroabsorption properties of *both* the p^+ layer (α_p''/ε_p) and of the intrinsic layer (α_i''/ε_i).

Once these coefficients are known, the built-in potential in the cell can be obtained using the following expression for normalized fundamental signal:

$$\frac{\delta T_{1f}/T}{C(V)\delta V}=-\frac{2\alpha_i''(\lambda)}{\varepsilon_i\varepsilon_0}\left\{\left(V-V_{bi}\right)+V_p\left(\frac{\alpha_p''(\lambda)/\varepsilon_p}{\alpha_i''(\lambda)/\varepsilon_i}-1\right)\right\} \tag{2}$$

We note that these expressions neglect thin-film interference effects in the films as well as "true" electroreflectance effects (due to the electric-field dependent refractive index of the films); we do not believe that incorporation of these corrections would significantly alter our conclusions.

Experimental Results on Cells with Microcrystalline *p* Layers

In the present work we present measurements on two cells deposited in the sequence *nip*. One cell (denoted "standard") has a conventional plasma-deposited a-Si:H intrinsic layer; the other (denoted "strong H dilution") has an intrinsic layer deposited using substantial hydrogen dilution of the silane feedstock gas. Both cells have a-Si:H n^+ layers and "microcrystalline" (μc-Si:H) p^+ layers. The open-circuit voltages under AM1.5 illumination were 0.93 V (standard cell) and 1.02 V (strong H-dilution) for the as-deposited state.

In Fig. 4 we have shown the measurements of the second harmonic electroabsorption modulation as a function of capacitance. The data are generated using the same 50 kHz fundamental modulation frequency and reverse bias range as for Fig. 1. The parameter ratios α_p''/ε_p and α_i''/ε_i are obtained as linear regression parameters from eq. (1). We present the fitting results for both types of cell in Fig. 5.

The standard and strongly hydrogen-diluted cells yield quite different spectra α_i''/ε_i for the intrinsic layers. The results on the standard intrinsic layer agree reasonably well with prior work on a-Si:H. The results for the hydrogen-diluted intrinsic layer presumably reflect the increased bandgap for this layer. The electroabsorption spectra of the microcrystalline p^+ layers in the two cells are similar, as would be expected given that these layers are nominally identical. It is nonetheless remarkable that this result emerged – considering the substantial differences in the magnitudes and wavelength dependence of the raw electroabsorption signals. The results suggest that the approximations in our heterostructure model are acceptable.

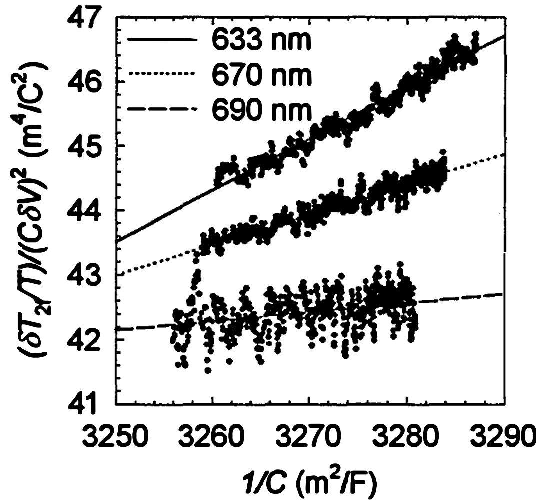

Fig. 4. Plot of the normalized, second harmonic electroabsorption signal δT_{2f} for three different wavelengths as a function of reciprocal capacitance in the standard cell; the data are generated by varying the reverse bias across the cell.

We estimated the built-in potentials in these two cells using the following procedure. We first plotted $(\delta T_{1f}/T)/(C(V)\delta V)$ as a function of bias voltage in order to obtain the voltage-axis intercept V_0. Representative measurements were presented in Fig. 1. V_0 depends slightly upon laser intensity, most likely due to photocharge stored in the samples. In Fig. 5, we have plotted V_0 for low intensities parametrically against the wavelength-dependent ratio $(\alpha''_p/\varepsilon_p)/(\alpha''_i/\varepsilon_i)$ (as obtained from Fig. 5). When this ratio is unity, the electroabsorption properties of the p^+ and intrinsic layers are the same. As a consequence, the value of the intercept interpolated for this value can be associated with the built-in potential (by the straightforward single-layer analysis). This qualitative argument is confirmed by equation (2).

As indicated in Fig. 5, we find V_{bi} = 0.98 V for the cell with the standard intrinsic layer, and V_{bi} = 1.25 V for the cell with the strong hydrogen dilution intrinsic. The result for the cell with a standard intrinsic layer and a microcrystalline *p* is similar to electroabsorption estimates of V_{bi} for cells with an a-SiC:H *p* layer. A review of estimates for V_{bi} using other techniques is beyond the scope of this paper.

Interface Dipole Hypothesis

The increase in V_{bi} for the strong-hydrogen dilution cell was surprising to us, since it is often assumed that the built-in potential in *pin* diodes should be determined by the Fermi levels of the n^+ and p^+ layers, and should be unaffected by the intrinsic layer interposed between them. This argument of course neglects the possible role of interfaces. We therefore speculate that our measurements are evidence for a significant *interface dipole* between the p^+ and intrinsic layers of a-Si:H based solar cells. By definition, such a dipole consists of compensating positive and negative electric charges separated by a distance comparable to the carriers' tunneling radii. We illustrated the effect of an interface dipole Δ in Fig. 3. The solid curves represent the band-bending without the dipole, and shows the effects of the conduction and valence band offsets ΔE_c and ΔE_v between the p^+ and intrinsic layer materials. The dashed curves include an interface dipole which reduces the band-bending and hence V_{bi}., increasing the apparent size of both band offsets.

The microscopic nature of such interface dipoles is mysterious, although they have been invoked for nearly 50 years in the context of the built-in potentials in Schottky barrier diodes on crystalline semiconductors and are included in textbook treatments of solar cell device physics. Sizable interface dipole effects (up to 0.7 eV) have been inferred in photoemission studies of the band offsets at the a-Si:H/a-$Si_{1-x}C_x$:H interface (Fang and Ley, 1989)

For the cells we have studied, it may be that a decrease in interface dipoles for the strongly H-diluted cell is the primary cause for the increase of about 0.1 V in its open-circuit voltage V_{OC} *vis a vis* the standard cell; the possibility is an alternative to attributing the increase in V_{OC} to an increase in the energy gap of the intrinsic layer. The interface dipole hypothesis also leads to some interesting suggestions beyond the electroabsorption measurements. For example, varying interface dipoles offers a rational explanation for the apparently contradictory estimates of band offsets from two independent internal photoemission experiments on c-Si/a-Si:H interfaces; one reported that the offset at the valence band was neglibible, and the other reported the conduction band offset as negligible (Mimura and Hatanaka, 1987; Cuniot and Marfaing, 1988). Finally, we speculate that part of the success of "buffer layers" at the p^+/i interface in increasing the open-circuit voltage V_{oc} in some a-Si:H based solar cells is due to modification of interface dipoles.

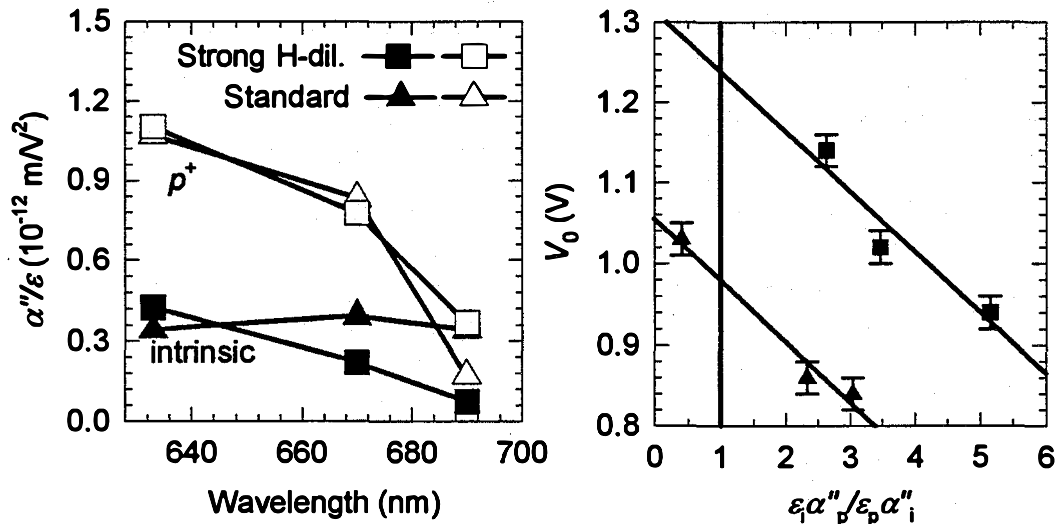

Fig. 5. *(left)* Electroabsorption coefficients α_i'' and α_p'' as a function of wavelength obtained for a-Si:H and for μc-Si:H:B respectively obtained in two types of cell (with standard and strongly H-diluted intrinsic layers). *(right)* Plot of the voltage-axis intercepts V_0 of first-harmonic electroabsorption measurements (obtained at three wavelengths) vs. the corresponding ratios of electroabsorption parameters $(\alpha_p''/\varepsilon_p)/(\alpha_i''/\varepsilon_i)$. The same two types of cells were used; the error bars indicate the standard deviation in V_0 for differing cells on the same substrate. The built-in potential is V_0 for $(\alpha_p''/\varepsilon_p)/(\alpha_i''/\varepsilon_i) = 1$ (cf. vertical line).

Heterostructure Model for Electroabsorption: Details

In this section we present a brief derivation of equations (1) and (2) given earlier. We only consider transmittance mode EA measurements; the extension to reflection mode (in which the illumination is reflected from a back-reflector and passes out through the top of the device) is straightforward but tedious.

As is well-known, the absorption coefficient in semiconductors is affected by the electrical field (E) inside the material and the wavelength (λ) of the incident light. Considering the symmetry of electroabsorption, only even order terms survive, so the lowest order expansion is:

$$\alpha(\lambda,E)=\alpha^0(\lambda)+\alpha''(\lambda)E^2. \tag{3}$$

We term $\alpha''(\lambda)$ the electroabsorption coefficient. In modulated electroabsorption measurements, a DC voltage V_{dc} is modulated by a high frequency AC voltage V_{ac}. For sufficiently high frequencies the electric field can be written:

$$E(x,t)=E_{dc}(x)+E_{bi}(x)+E_{ac}\sin\omega t\,; \tag{4}$$

ω is the angular frequency of the modulation, and x, t for position and time respectively. Although the DC and built-in fields are position dependent, we have assumed that the modulated field is uniform (corresponding to the use of a large modulation frequency). The electric-field dependent transmittance through a homogeneous layer of thickness d may be written $T(E)=T_0\exp\left(-\int_0^d \alpha''(\lambda)E^2dx\right)$; where $T_0=I_0e^{-\alpha^0(\lambda)d}$. Assuming that the electroabsorption is weak, we expand the exponential $e^{-y}\approx 1-y$, obtaining:

$$T=T_0\left\{1-\int_0^d \alpha''(\lambda)\left[\left(E_{dc}+E_{bi}\right)^2+\frac{E_{ac}{}^2}{2}+2\left(E_{dc}+E_{bi}\right)E_{ac}\sin\omega t-\frac{1}{2}E_{ac}^2\cos 2\omega t\right]dx\right\} \tag{5}$$

So the normalized first harmonic signal is

$$\frac{\delta T_{1f}}{T}=-\int_0^d \alpha''(\lambda)2\left(E_{dc}+E_{bi}\right)E_{ac}dx, \tag{6}$$

and the second harmonic signal is:

$$\frac{\delta T_{2f}}{T}=\frac{1}{2}\int_0^d \alpha''(\lambda)E_{ac}^2dx. \tag{7}$$

If only a single intrinsic layer is involved in electroabsorption, we can re-express eq. (6) in terms of the capacitance C at the modulation frequency and the modulation voltage V_{ac}. We obtain:

$$\frac{\delta T_{1f}}{T}\frac{\varepsilon_i\varepsilon_0 A}{2V_{ac}C}=-\alpha_i''(\lambda)\left(V_{dc}+V_{bi}\right)\ ; \tag{8}$$

where ε_i indicates the dielectric constant of the layer. As expected, the voltage intercept of the signal is the built-in potential; the second harmonic signal is independent of the DC potential:

$$\frac{\delta T_{2f}}{T} = \frac{1}{2}\alpha_i''(\lambda)\frac{V_{ac}^2}{d_i} . \tag{9}$$

To extend this approach to include electroabsorption both from the p^+ and intrinsic layer, we use the approximation of a depletion zone in the p^+ layer of width d_p, as indicated in Fig. 3. As the reverse bias on the structure increases, the space charge and potential drop V_{dc}^p in the p^+ layer increases as illustrated (for V_{dc}). Increasing reverse bias also increases the "depletion zone" width d_p which is probed by high-frequency measurements. In this model the capacitance is dependent (slightly) upon reverse bias; considering the differences of dielectric constant of two layers and the continuity of electrical displacement vector at the *p/i* interface, d_p, can be expressed in terms of the capacitance C per unit area as:

$$d_p = \frac{\varepsilon_p \varepsilon_0}{C} - \frac{\varepsilon_p}{\varepsilon_i} d_i . \tag{10}$$

The *1f* signal now becomes:

$$\frac{\delta T_{1f} / T}{C(V)\delta V} = -\frac{2\alpha_i''(\lambda)}{\varepsilon_i \varepsilon_0}\left\{\left(V - V_{bi}\right) + V_p\left(\frac{\alpha_p''(\lambda)/\varepsilon_p}{\alpha_i''(\lambda)/\varepsilon_i} - 1\right)\right\} . \tag{11}$$

where we have separated the built-in potential V_{bi}, into its components V_p and V_i across the p^+ and intrinsic layers, respectively. We have also redefined V_{ac} as δV to re-establish consistency with our earlier equations 1 and 2.

Note that when the "electroabsorption ratio" $\varepsilon_i \alpha_p''(\lambda) / \varepsilon_p \alpha_i''(\lambda)$ is unity, the standard analysis of EA measurements yields the correct V_{bi}, $= V_{bi}^i + V_{bi}^p$; this was previously suggested by Wang, *et al* (1994) on purely physical grounds, since the 2 distinct layers then have identical electroabsorption properties.

The difficulty has been to find a procedure for ascertaining this electroabsorption ratio. We have found that the second harmonic (*2f*) measurements can be used to do this. From eq.(9) and eq.(10), the *2f* signal can be expressed as:

$$\frac{\delta T_{2f} / T}{(C(V)\delta V)^2} = \frac{\left(\alpha_p''(\lambda)/\varepsilon_p\right)}{2\varepsilon_0 C(V)} + \frac{\left(\alpha_i''(\lambda)/\varepsilon_i - \alpha_p''(\lambda)/\varepsilon_p\right)}{2\varepsilon_0\left(\varepsilon_i \varepsilon_0 / d_i\right)} . \tag{12}$$

On the right side of Eq. (10), only the capacitance C changes with V_{dc}.

The importance of this expression is that, unlike eq. (9), we do not need to know the division of the electric potential between the p^+ and intrinsic layers in order to use it. A fitting of the measurements to the voltage-dependent capacitance yields both α_p'' and α_i'' as fitting parameters.

Hole Drift Mobility in Hydrogenated Amorphous Silicon Deposited Using the Hot-Wire Method

We have measured hole photocarrier drift-mobilities on hydrogenated amorphous silicon (a-Si:H) deposited using the hot-wire method. The material contains about 2 atomic percent hydrogen, which is much lower than for "standard" plasma-deposited a-Si:H. Under comparable conditions we find hole mobilities as large as 10^{-2} cm^2/Vs at room temperature, about five times larger than for standard a-Si:H. Temperature-dependence measurements were consistent with the valence bandtail trapping model for these mobilities. In conjunction with recent work of Ganguly and Matsuda on triode-deposited a-Si:H, these results on hot-wire a-Si:H indicate that significant improvements in hole mobilities are achievable in a-Si:H.

Introduction

The low drift mobility of holes is an important limitation to amorphous silicon based materials, and there have been many efforts to find deposition processes which would improve it. The hole mobilities are limited by trapping processes involving the valence bandtail. Remarkably, for the entire class of plasma-deposited amorphous silicon-germanium and amorphous silicon-carbon alloys deposited in "diode" reactors, representing many years of materials research, it has been found that the hole drift mobility remains nearly constant, with a best value of 2×10^{-3} cm^2/Vs under standard conditions (Gu, Wang, Schiff, Li, and Malone, 1994, and references therein).

There have been several indications recently that this apparent limit to the hole drift mobility of a-Si:H based materials may be surmounted. In particular Ganguly and Matsuda (1995) have reported much larger values for the hole mobility in a-Si:H deposited under carefully chosen conditions in a "triode" reactor. This work has not yet been confirmed by other laboratories. In the present Letter we present hole drift mobility measurements in a-Si:H deposited using the "hot-wire" technique. Although there is a significant range of hole mobilities in these specimens, we have measured values as large as 10^{-2} cm^2/Vs, five times the value for conventional a-Si:H alloys.

Time-of-Flight Measurements

Specimens and Instruments

The measurements reported in this Letter were obtained on a 2.3 μm hot-wire layer deposited onto stainless steel, forming a Schottky barrier structure. A 40 nm n^+ a-Si:H top layer was plasma-deposited onto the hot-wire layer, and a thin Pd film evaporated onto the n^+ layer. The structure was prepared at the National Renewable Energy Laboratory (NREL). Descriptions of the hot-wire deposition procedures and of additional structural and transport characterizations have been given elsewhere (Mahan and Vanecek, 1991; Crandall, 1992). Here we restrict ourselves to noting that the hot-wire material used in the present study is amorphous (based on Raman measurements), has about 2 atomic % of hydrogen and a "Tauc" bandgap of 1.60 eV. The thickness was measured on a co-deposited substrate using a mechanical profilometer. Specimens were studied in their as-deposited state without extensive light exposure.

Time-of-flight measurements were done using a transient photocurrent apparatus; the procedures have been described in detail elsewhere (Wang, Antoniadis, Schiff, and Guha, 1993). We used a pulsed laser tuned to a wavelength of 590 nm, for which we estimate that carrier generation occurred within about 1000 Å of the (top) illuminated Pd/n^+ interface.

Time-of-flight measurements

In this section we present measurements on the diode which gave the largest hole drift mobility. In Fig. 6 we present normalized photocurrent transients $i(t)d^2/Q_0V$ for several temperatures and a uniform field of V/d = 69.5 kV/cm. d is the i-layer thickness, V is the applied voltage, and Q_0 is the photocharge generated in the structure. The normalization eliminates any linear dependence of the photocurrent upon applied bias voltage or laser intensity.

The voltage polarity corresponds to hole transit across the structure. The photocharge Q_0 was estimated by integrating the transient photocurrent $i(t)$. Q_0 varied about 30% with temperature, which we attribute to the temperature-dependent absorption of the n^+ layer.

The transients have the qualitative form expected for holes in a-Si:H. Consider the lowest curve, corresponding to 200 K. After an initial "peak," one sees a shallow decay commencing around 2×10^{-7} s. We identify this as the classical, dispersive behavior of the drifting holes prior to the onset of effects due to their sweepout at the opposing electrode. Commencing around 3×10^{-5} s, this transient steepens, which corresponds to the "post-transit" regime of dispersive transport. Similar effects can be discerned for all temperatures, although the present figure makes detailed separation of the current transients for differing temperatures somewhat difficult.

In addition to this well-known dispersive form for the transient photocurrent at longer times, Fig. 6 reveals a relatively temperature-independent peak at the earliest times ($t < 100$ ns). We attribute this to electron transit across the photogeneration region (first 1000 Å in the n-layer side). The time-scale of this signal is determined by the capacitance of the diode in conjunction with the 50 Ohm impedance of the electronics and cables.

Time-of-flight estimates of a drift mobility μ_D are based on the expression:

$$\mu_D = L/E\, t_T$$

where L is the average dispacement of the photocarriers at the transit time t_T, and E is the (uniform) applied electric field. Dispersive photocarrier transport implies that this drift mobility depends strongly upon the ratio L/E.

In order to compare the mobilities from different materials it is essential to specify a particular value for L/E which must be used for all specimens (Wang, *et al*, 1993). To obtain the transit times corresponding to a standard value of L/E, we integrate the normalized photocurrents in Fig. 6; this yields a plot of L/E vs. t, as shown in the lower portion of Fig. 6. The tendency of the charge plots to saturate around 3×10^{-9} cm^2/Vs corresponds to sweepout: the maximum displacement of a hole is the sample thickness of 2.3 μm, so for the present plot the maximum value of $L/E = 3.4\times10^{-9}$cm^2/Vs.

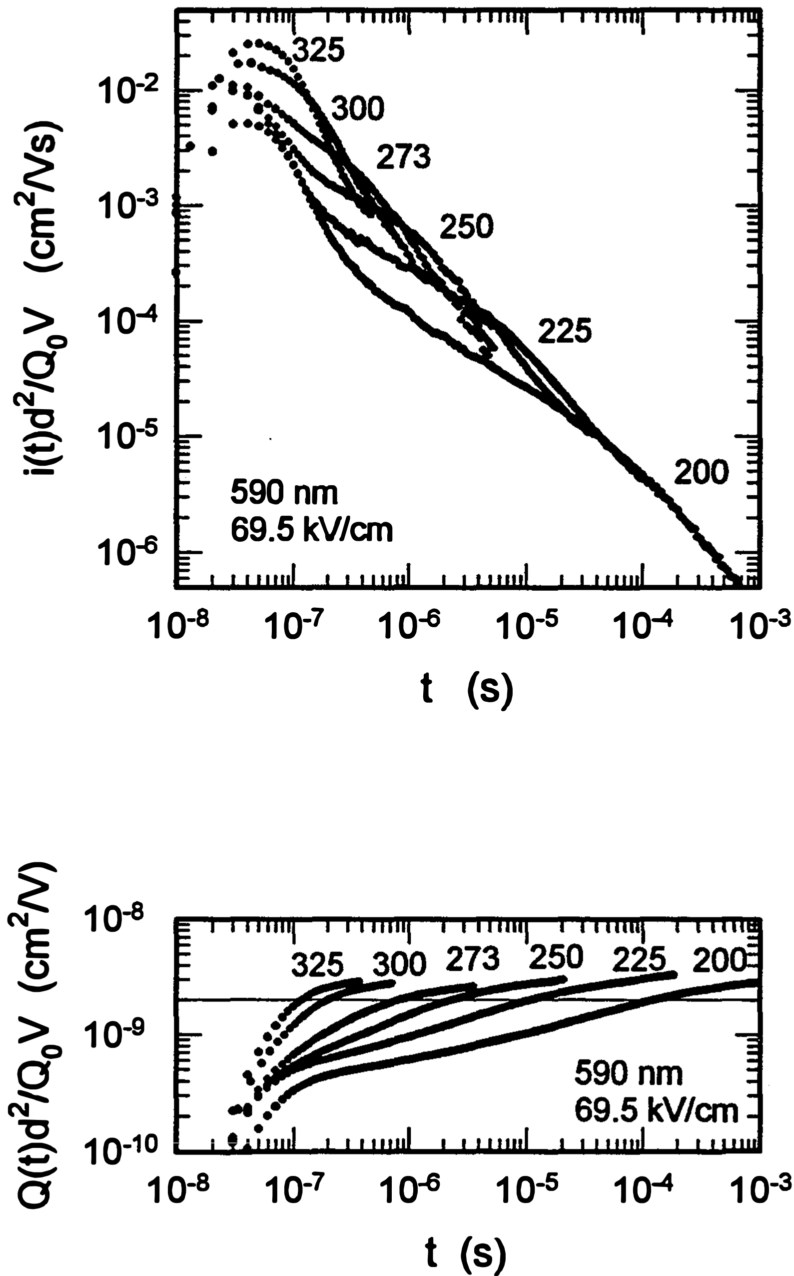

Fig. 6. (upper) Normalized transient photocurrents $i(t)d^2/Q_0V$ for holes measured at λ = 590 nm at several temperatures and constant electric field of 69.5 kV/cm. (lower) Logarithmic plot of $Q(t)d^2/Q_0V$ for the same conditions as the transients; for times sufficiently early that carriers have not yet been swept completely across the structure, the charge transient measures the time dependence of $L(t)/E$ of the hole displacement $L(t)$ to the electric field E. The intersection of each curve with the line at 2×10^{-9} cm^2/V determines the transit times used to calculate a standard drift mobility.

We chose a "standard" value of $L/E = 2 \times 10^{-9}$ cm^2/V for reporting μ_d, which corresponds to transit across a structure of thickness 0.6 μm at 0.9 V applied bias. $L/E = 2 \times 10^{-9}$ cm^2/V was also used in previous work on electron transport in a-SiC:H and a-SiGe:H by Wang, *et al* (1993a, 1993b) and for hole transport by Gu, *et al* (1994). The horizontal line in the lower portion of Fig. 6 indicates this value for L/E; the transit times used for computing μ_D are obtained from the intersection of this line with the measured $Q(t)$ curves at various temperatures.

Results

As a summary of our experiment, in Fig. 7 we have plotted the measured hole drift mobilities μ semilogarithmically against reciprocal temperature $1/T$. We show results at two values of L/E for the "best" hot-wire specimen. We also show previously published hole drift mobility measurements from our laboratory (Gu, *et al*, 1994) on a "standard" a-Si:H sample prepared at Energy Conversion Devices, Inc. using a diode-type plasma deposition reactor. These measurements on "standard" a-Si:H are consistent with completely independent work from at least two other laboratories. The hole mobilities measured for the HW a-Si:H specimen are significantly higher than the measurements on conventional a-Si:H.

The solid lines in Fig. 7 are our fits to the measurements using the exponential bandtail multiple-trapping model for the hole drift mobility:

$$\mu_D = \mu_0 \left({Lv}/{\mu_0 E} \right) \left[{Lv}/{\mu_0 E} \right]^{-E_0/kT} \quad (13)$$

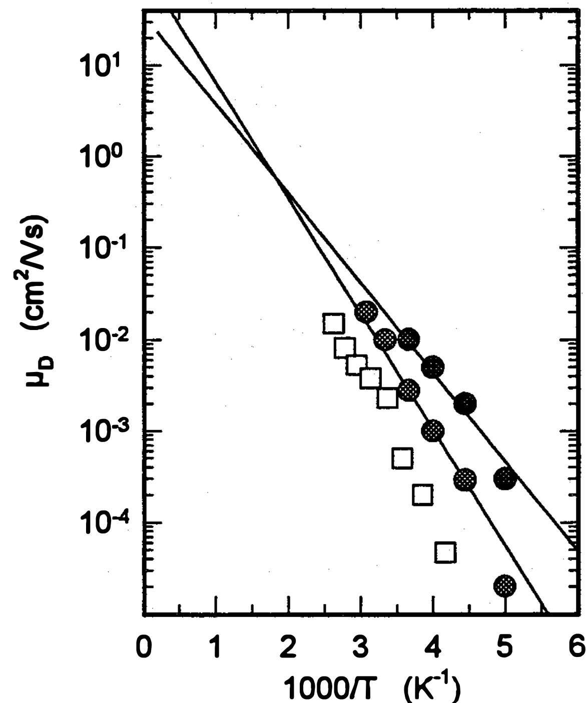

Fig. 7. Semilogarithmic plot of average hole drift mobility μ as a function of reciprocal temperature $1/T$. for a displacement/field ratio of $L/E = 2\times10^{-9}$ cm^2/V. Two solid lines are a multiple-trapping fit. Open symbols represent the result from an optimized a-Si:H sample.

where E_0 is the characteristic energy of the exponential valence bandtail, μ_0 is the "microscopic" mobility of holes, and ν is an "attempt-to-escape" frequency for holes trapped in the valence bandtail. The multiple-trapping model gives an acceptable fit. Unfortunately, no single parameter accounts for the increase in the hole mobility in the hot-wire material. Additional measurements at higher temperatures and for a larger range of *L/E* values would probably clarify this issue, but we were unable to execute such measurements in the present specimens.

In Fig. 8 we have plotted the correlation of hole drift mobility measurements with the optical bandgap for a variety of specimens at room-temperature under the standard condition $L/E = 2\times10^{-9}$ cm^2/Vs . The cluster of solid symbols at 1.6 eV represents numerous measurements on hot-wire a-Si:H; we have found considerable variability in our measurements. We believe this represents an underlying variability in the hot-wire materials since we have generally obtained much narrower variance for standard a-Si:H. On the figure we have also indicated using an arrow the very large hole mobilities measured by Ganguly, *et al* in triode-deposited a-Si:H; it is probably worth noting that these authors also report considerable variability in their hole measurements.

We comment briefly on whether the relatively large hole mobilites we have measured could have been inferred from earlier measurements of large hole diffusion lengths in similar materials. We note that neither parameter can be predicted from the other. In recent work Schwarz, *et al* have shown that diffusion length measurements in "standard" a-Si:H can be predicted from knowledge of *both* the hole drift mobility (as a function of *L/E*) and the recombination response time. It is likely that improved hole drift mobilities may play a role in the improved diffusion length, but a complete understanding of the latter requires an understanding of electron-hole recombination as well as of hole transport.

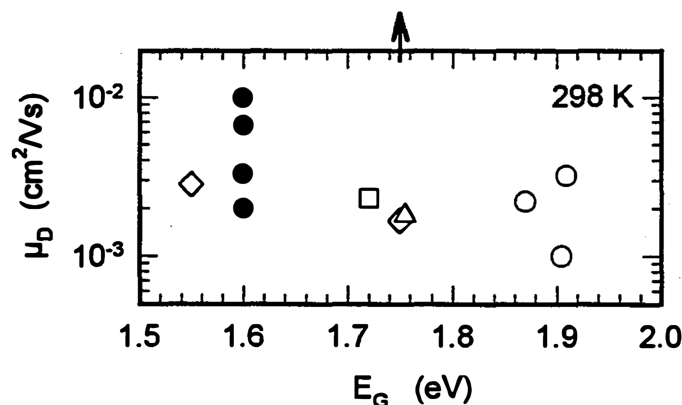

Fig. 8. Summary of hole drift mobility at 298 K evaluated at $L/E = 2\times10^{-9}$ cm^2/V as a function of bandgap. The highest points are reported recently by Ganguly *et al.*

Relationship of Ambipolar Diffusion Length Measurements and Hole Drift Mobilities in a-Si:H

The ambipolar diffusion-length L_{amb} is one of the measured properties of an a-Si based material used to infer photovoltaic quality. The interpretation of this parameter is well-known to semiconductor device scientists; roughly, the parameter indicates how far the *less mobile* carrier in a semiconductor diffuses before it recombines with the more mobile carrier.

The strong interest in L_{amb} in recent years has occurred because of the development of a simple experimental technique for measuring it. This is the *steady state photocarrier grating* measurement developed by Ritter, Zeldov, and Weiser (1986). It has been used for this purpose in the development of hot-wire a-Si:H at NREL, of a-SiC:H at Solarex, and elsewhere. Despite this popularity, there is little understanding of the meaning of L_{amb}, so its success as a photovoltaic materials quality factor is based on phenomenological correlations.

The importance of our work for photovoltaic properties is the following. There are several plausible recombination channels for holes in a-Si:H which are, for example, all incorporated into standard device models such as AMPS. The advance we have made is that we can subject each channel to a very severe, quantitative constraint: the ambipolar diffusion length must agree numerically with estimates of the hole drift mobility and the Einstein relation $D = (kT/q)\mu$ of diffusion constant and mobility.

The particular model for which we obtain agreement is illustrated in Fig. 9. The curve labeled "drift" is compatible with hole time-of-flight measurements in a-Si:H (Tiedje, 1984; Gu, *et al*, 1994b). It shows the function $x(t)$ indicating how far a hole drifts under the influence of an electric field as a function of time; the particular form for $x(t)$ is apparently dictated by multiple-trapping in the valence bandtail (Tiedje, 1984).

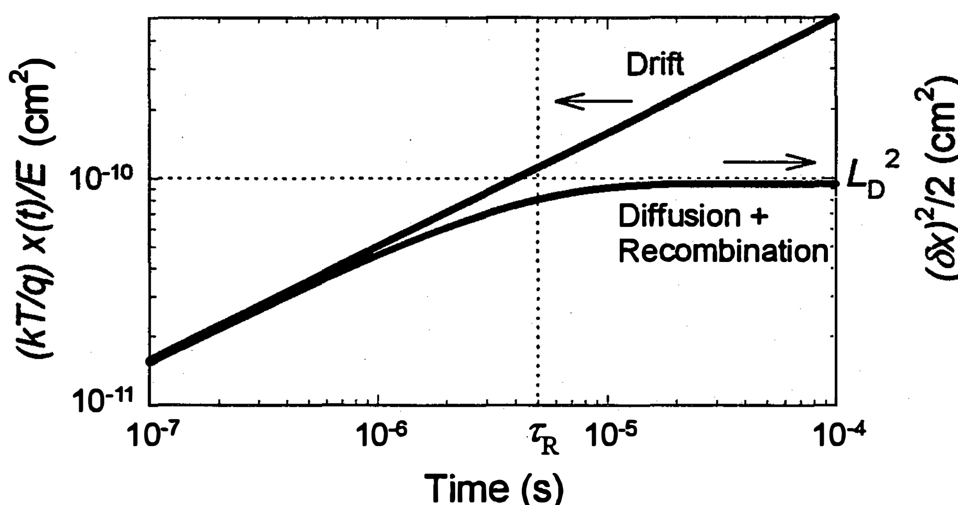

Fig. 9: Proposed model for the relationship of hole drift and diffusion measurements. Drift measurements are made under recombination free conditions; diffusion measurements usually yield only the diffusion length L_D, which is determined by the hole diffusion truncated at the recombination time τ_R.

The curve labeled "diffusion and recombination" is a reasonable model for the mean-square diffusion $(\delta x)^2$ of a hole as a function of time: Given the Einstein relation, the normalized hole diffusion should agree with the time-of-flight measurement at short times (the bandtail multiple-trapping regime). At longer times, after an electron annihilates the hole near a recombination response time τ_R, the diffusion approaches the diffusion length L_D. Note that this view neglects the "deep-trapping" by a dangling bond prior to recombination.

In Fig. 10 we show the correlation of the measured average diffusion constant D with the average mobility μ. These results were obtained on several intrinsic a-Si:H materials prepared by plasma-deposition at the Technical University of Munich and at Syracuse University.

The average diffusion constant is obtained from SSPG and photoconductivity response time measurements on thin films deposited onto glass with coplanar metal contacts (see Wang and Schwarz, 1994 for details; the actual measurements are presented in Gu, Schiff, Grebner, Wang, and Schwarz, 1996). In particular we evaluate as $D_h = L_{amb}^2 / 2\tau_R$, where L_{amb} is the ambipolar diffusion length actually measured by SSPG and τ_R is the recombination response time measured from the photoconductivity decay time. Note that D_h depends upon the illumination intensity used for the measurements.

The average mobility is based on the function $x(t)/E$ measured in time-of-flight for holes; these measurements are conducted under near-dark conditions, and are reported in Gu, *et al*, 1996. The mobility is then calculated using $x(t)/E$ as evaluated at the same response times used to calculate D_h: $\mu_h = x(\tau_R)/E\tau_R$.. The TOF measurements were done on Schottky barrier structures; the a-Si:H films were co-deposited with the coplanar electrode samples used for SSPG. Remarkably, the completely different experiments yield results which are consistent with the Einstein relation over some three orders of magnitude. We believe that

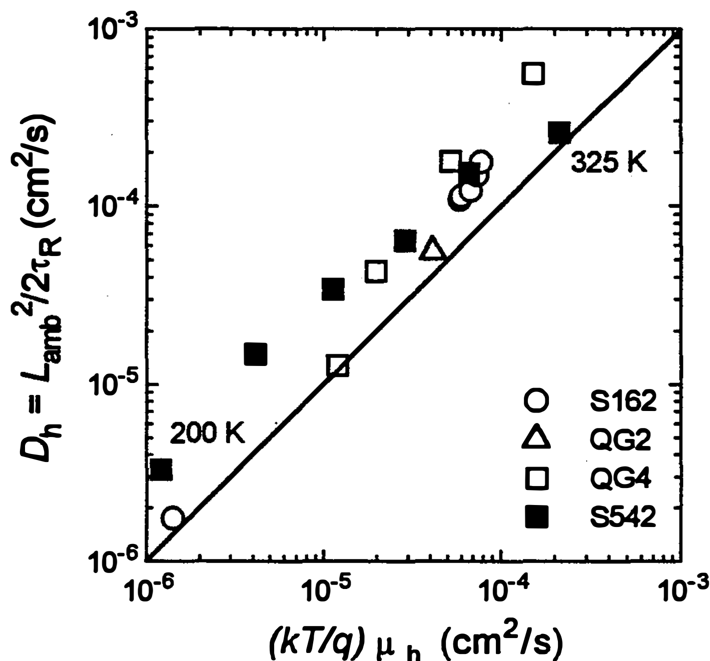

Fig. 10. Correlation of the hole diffusion coefficient D_h with the "Einstein normalized" hole drift mobility $(kT/q)\mu_h$; both are averaged from their photogeneration up to recombination at time τ_R. Measurements for four specimens over a range of temperatures and illumination intensities are indicated. The Einstein relation $D_h = (kT/q)\mu_h$ is indicated by the solid line.

the remaining discrepancy is due to some approximations in the standard analysis of the ambipolar diffusion length measurement (Ritter, Zeldov and Weiser, 1988; Wang and Schwarz, 1994). A discussion of the more general theoretical situation is given in the published article presenting this work (Gu, Schiff, Grebner, Wang, and Schwarz, 1996).

One other interesting fact -- other than the probable validity of the Einstein relation -- can be deduced from these results. Hole deep-trapping has been measured using time-of-flight techniques (see Liu, Maruyama, Wagner, and Delahoy, 1989, for some measurements); this process most likely corresponds to the capture of a hole by a dangling bond at sufficiently long times. Since time-of-flight is done under near dark conditions, it is unclear whether a hole is also "deep-trapped" prior to its recombination under normal solar illumination conditions. The results we have just presented show that ambipolar diffusion under solar illumination conditions is complete at times prior to hole deep trapping; in other words, annihilation of holes by electrons occurs before the holes are deep-trapped in a-Si:H under reasonable illumination intensities.

References

I. H. Campbell, M. D. Jowick, and I. D. Parker, *Appl. Phys. Lett.* **67**, 3171 (1995).

R. S. Crandall, *in Photovoltaic Advanced Research & Development Project* : *AIP Conference Proceedings No. 268*, edited by R. Noufi (American Institute of Physics, New York, 1992), p. 81.

M. Cuniot and Y. Marfaing, *Phil. Mag. B* **57**, 291 (1988).

R.-C. Fang and L. Ley, *Phys. Rev. B* **40**, 3818 (1989).

S. J. Fonash, *Solar Cell Device Physics* (Academic, New York, 1981) .

G. Ganguly and A. Matsuda, in *Amorphous Silicon Technology-1994*, edited by E. A. Schiff, *et al* (Materials Research Society, Symposium Proceedings Vol. 336, Pittsburgh, 1994), p. 7.

Qing Gu, Qi Wang, E. A. Schiff, Y. M. Li and C. T. Malone, J. Appl. Phys. **76**, 2310 (1994).

Qing Gu, E. A. Schiff, S. Grebner, F. Wang, and R. Schwarz, *Phys. Rev. Lett.* **76**, 3196 (1996).

S. Guha, J. Yang, P. Nath, and M. Hack, *Appl. Phys. Lett.* 49, 218 (1986).

S. Guha, J. S. Payson, S. C. Agarwal and S. R. Ovshinsky, *J. Non-Cryst. Solids* **97&98**, 1455 (1987).

L. Jiang and E. A. Schiff, in *Amorphous Silicon Technology-1996*, edited by M. Hack, *et al* (Materials Research Society, Symposium Proceedings Vol. 420, Pittsburgh, 1996), *in press.*

L. Jiang, Q. Wang, E. A. Schiff, S. Guha, J. Yang, and X. Deng, *unpublished.*

J. Z. Liu, A. Maruyama, S. Wagner, and A. Delahoy, *J. Non-Cryst. Solids* **114**, 453 (1989).

A. H. Mahan and M. Vanecek, in *Amorphous Silicon Materials and Solar Cells*, edited by B. L. Stafford (American Institute of Physics, New York, 1991), p. 195.

H. Mimura and Y. Hatanaka, *Appl. Phys. Lett.* **50**, 326 (1987).

S. Nonomura, H. Okamoto, and Y. Hamakawa, *Appl. Phys. A* **32**, 31 (1983).

E. H. Rhoderick, *Metal-semiconductor Contacts* (Oxford, New York, 1988).

D. Ritter, E. Zeldov, and K. Weiser, *Appl. Phys. Lett.* **49**, 791 (1986).

D. Ritter, E. Zeldov, and K. Weiser, *Phys. Rev. B* **38**, 8296 (1988).

T. Tiedje, in *Hydrogenated Amorphous Siliocn II*, edited by J. D. Joannopoulos and G. Lucovsky (Springer, New York, 1984), pp. 261-300.

R. Vanderhaghen and C. Longeaud, *J. Non-Cryst. Solids* **114**, 540(1989).

F. Wang and R. Schwarz, *Appl. Phys. Lett.* **65**, 884 (1994).

Qi Wang, Homer Antoniadis, E. A. Schiff and S. Guha, *Phys. Rev. B*, **47**, 9435 (1993).

Qi Wang, E. A. Schiff and Y. M. Li, in *Amorphous Silicon Technology-1993*, edited by E. A. Schiff, M. J. Thompson, A. Madan, K. Tanaka and P. G. LeComber, (Materials Research Society, Symposia Proceedings No. 297 Pittsburgh, 1993), p. 803.

Q. Wang, E. A. Schiff, and S. S. Hegedus, in *Amorphous Silicon Technology-1994*, edited by E. A. Schiff, *et al* (Materials Research Society, Symposium Proceedings Vol. 336, 1994), p. 365.

REPORT DOCUMENTATION PAGE

Form Approved
OMB NO. 0704-0188

Public reporting burden for this collection of information is estimated to average 1 hour per response, including the time for reviewing instructions, searching existing data sources, gathering and maintaining the data needed, and completing and reviewing the collection of information. Send comments regarding this burden estimate or any other aspect of this collection of information, including suggestions for reducing this burden, to Washington Headquarters Services, Directorate for Information Operations and Reports, 1215 Jefferson Davis Highway, Suite 1204, Arlington, VA 22202-4302, and to the Office of Management and Budget, Paperwork Reduction Project (0704-0188), Washington, DC 20503.

1. AGENCY USE ONLY (Leave blank)	2. REPORT DATE	3. REPORT TYPE AND DATES COVERED
	January 1997	Annual Technical Progress Report, 15 May 1995 - 15 May 1996

4. TITLE AND SUBTITLE

Research on High-Bandgap Materials and Amorphous Silicon-Based Solar Cells; Annual Technical Progress Report, 15 May 1995 - 15 May 1996

5. FUNDING NUMBERS

C: XAN-4-13318-06
TA: PV704401

6. AUTHOR(S)

Schiff, E.A.; Gu, Q.; Jiang, L.; Rao, P.

7. PERFORMING ORGANIZATION NAME(S) AND ADDRESS(ES)

Syracuse University
Syracuse, New York 13244-1130

8. PERFORMING ORGANIZATION REPORT NUMBER

9. SPONSORING/MONITORING AGENCY NAME(S) AND ADDRESS(ES)

National Renewable Energy Laboratory
1617 Cole Blvd.
Golden, CO 80401-3393

10. SPONSORING/MONITORING AGENCY REPORT NUMBER

SR-520-22362

DE97000102

11. SUPPLEMENTARY NOTES

NREL Technical Monitor: B. von Roedern

12a. DISTRIBUTION/AVAILABILITY STATEMENT

12b. DISTRIBUTION CODE

UC-1260

13. ABSTRACT *(Maximum 200 words)*

In this report, the researchers present a technique for using modulated electroabsorption measurements to determine the built-in potential in semiconductor heterojunction devices. The technique exploits a simple relationship between the second-harmonic electroabsorption signal and the capacitance of such devices. The researchers apply this technique to hydrogenated amorphous silicon (a-Si:H) based solar cells incorporating microcrystalline Si p^+ layers. For one set of cells with a conventional plasma-deposited intrinsic layer, they obtain a built-in potential of 0.98±0.04V; for cells with an intrinsic layer deposited using strong hydrogen-dilution, they obtain 1.25±0.04 V. The researchers speculate that interface dipoles between the p^+ and intrinsic layers significantly influence the built-in potential.

14. SUBJECT TERMS

solar cell built-in potential ; amorphous silicon-based solar cells ; high-bandgap materials ; electroabsorption ; hydrogenated amorphous silicon

15. NUMBER OF PAGES
25

16. PRICE CODE

17. SECURITY CLASSIFICATION OF REPORT	18. SECURITY CLASSIFICATION OF THIS PAGE	19. SECURITY CLASSIFICATION OF ABSTRACT	20. LIMITATION OF ABSTRACT
Unclassified	Unclassified	Unclassified	UL